ISSN 0965-5425, Computational Mathematics and Mathematical Physics, 2025, Vol. 65, No. 7, pp. 1453–1471. © Pleiades Publishing, Ltd., 2025.

GENERAL NUMERICAL METHODS

Dedicated to Eugene Tyrtyshnikov on the occasion of his 70th anniversary

Eigenvalues of Non-Hermitian Banded Toeplitz Matrices Approaching Simple Points of the Limiting Set

M. Bogoya[a,*] and S. M. Grudsky[b,c,]**

[a] *Universidad del Valle, Department of Mathematics, Cali, 760001 Colombia*

[b] *CINVESTAV-IPN, Department of Mathematics, CDMX, 07360 Mexico*

[c] *Southern Federal University, Regional Mathematical Center, Rostov-on-Don, 344006 Russia*

** e-mail: johan.bogoya@correounivalle.edu.co*

*** e-mail: grudsky@math.cinvestav.mx*

Received February 27, 2025; revised April 15, 2025; accepted April 15, 2025

Abstract—For large non-Hermitian banded Toeplitz matrices, it is well known that their eigenvalues cluster along a limiting set, which is formed by a finite union of closed analytic arcs. We consider general non-Hermitian banded Toeplitz matrices and extend the simple-loop method to obtain individual asymptotic expansions for eigenvalues approaching simple and non-degenerate points of the limiting set as the matrix order increases to infinity. We also develop an algorithm to effectively compute these expansions.

Keywords: Toeplitz matrix, asymptotic expansion, eigenvalues, simple loop method

DOI: 10.1134/S0965542525700745

1. INTRODUCTION

Let a be a function in $L^\infty(\mathbb{T})$, where $\mathbb{T} = \partial\mathbb{D}$ is the boundary of the unit complex disc. We denote by $T_n(a)$ the $n\times n$ Toeplitz matrix $(a_{j-k})_{j,k=0}^{n-1}$,

$$\begin{pmatrix} a_0 & a_{-1} & & a_{-n+1} \\ a_1 & a_0 & a_{-1} & \\ & a_1 & a_0 & \ddots \\ & & \ddots & \ddots & a_{-1} \\ a_{n-1} & & & a_1 & a_0 \end{pmatrix},$$

where a_k stands for the kth Fourier coefficient of a, that is

$$a_k = \frac{1}{2\pi}\int_{-\pi}^{\pi} a(e^{i\sigma})e^{-ik\sigma}d\sigma.$$

As we can see, the matrix $T_n(a)$ has constant entries along the main diagonals. The function a is usually called *symbol* or *generating function*.

Due to their wide range of applications, Toeplitz matrices have been a subject of sustained interest for over a century. In particular, the study of their spectral properties—including spectral distribution, clustering, localization, and the behavior of eigenvalues and eigenvectors—has generated a vast body of literature. See the brilliant and beautiful paper [1] of E. Tyrtyshnikov for a compendium and unifying results about spectral distribution, localization, and clustering. Further general and in-depth treatments of Toeplitz operators and matrices can be found in [2–4].

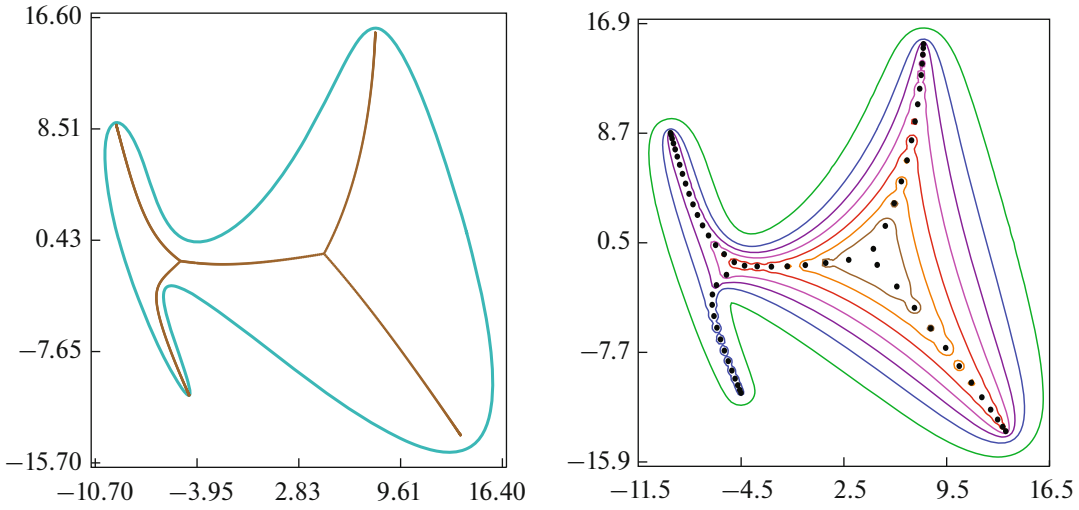

Fig. 1. (Left) The range (green curve) and the limiting set (brown curve) for the symbol $a(t) = -t^{-4} - (3 + 2\mathrm{i})t^{-3} + \mathrm{i}t^{-2} + t^{-1} + 10t + (3 + \mathrm{i})t^2 + 4t^3 + \mathrm{i}t^4$. (Right) The ε-pseudospectrum of $T_n(a)$. The black points are the eigenvalues of $T_{64}(a)$ while the green to brown curves correspond to $\varepsilon = 1/15, 1/30, \ldots, 1/90$, respectively. This example is called the "whale" and was treated in [6], where a picture similar to the left one appears on the title page. The limiting set was computed using the algorithm in [7].

The spectral study of Toeplitz matrices naturally divides into two cases: Hermitian and non-Hermitian. The former case has been extensively studied and, in general, is well understood. But besides a number of related articles, it is fair to say that the latter case is more complicated and less clear.

The matrix $T_n(a)$ is Hermitian if and only if a is real-valued. Therefore, to study the non-Hermitian case we need to focus on truly complex-valued symbols.

Let a be a Laurent polynomial, that is,

$$a(t) = a_{-r}t^{-r} + a_{-r+1}t^{-r+1} + \ldots + a_{\ell-1}t^{\ell-1} + a_\ell t^\ell, \tag{1.1}$$

where $a_j \in \mathbb{C}$ for $j = -r, \ldots, \ell$ and $a_{-r}a_\ell \neq 0$. The cases $r \leqslant 0$ and $\ell \leqslant 0$ produce trivial spectra, hence we assume that $r, \ell \geqslant 1$. In 1960 P. Schmidt and F. Spitzer [5] showed that, as n increases to infinity, the spectra $\operatorname{sp} T_n(a)$ converge in the Hausdorff metric to a certain limiting set $\Lambda(a)$, which is the union of finitely many analytic arcs, see Fig. 1.

For a symbol a with the form (1.1), the respective matrix $T_n(a)$ has a finite number of non-zero diagonals. In such a case we say that it is a *banded Toeplitz matrix*.

The findings in [5] were among the first to achieve a degree of generality in the non-Hermitian case. However, they provided no description of how to find those arcs, nor even how many of them $\Lambda(a)$ contains. It was only with the work of [8] that the connectedness of $\Lambda(a)$ was established.

For a banded Toeplitz matrix, the eigenvector matrix of $T_n(a)$ is, in general, severely ill conditioned. Hence, the numerical computation of its eigenvalues is a challenging task (see the related discussion in the introduction of [9]). To see that, consider the well-known ε-pseudospectrum of a matrix A given by

$$\operatorname{sp}_\varepsilon(A) = \left\{\lambda \in \mathbb{C} : \left\|(A - \lambda I)^{-1}\right\| > 1/\varepsilon\right\}.$$

For small values of ε, let's say $\varepsilon = 1/50$, we expect that $\operatorname{sp}_\varepsilon(A)$ separates the eigenvalues of A. But if it is not, then an reliable numerical calculation of those eigenvalues will require a large number of precision digits, memory, and processing time. Figure 1 shows the ε-pseudospectrum for an iconic example. There we can see that the eigenvalues near the central part are impossible to approximate using machine precision. For instance, to obtain those eigenvalues in the software Julia v.1.9.2 for $n = 2048$ with 16 correct decimal digits, it was necessary to compute them using 2048-bit BigComplexFloat data type, which is equivalent to 660 digits of precision. The process took 16 days and consumed 1.8 TB of memory in a supercomputer.

The study of eigenvalue distributions – understood as the probability density describing their spread across the complex plane – evolved until the 1996 celebrated paper [1], which marked a culmination of that research branch.

In 2010, the work [10] considered a class of Hermitian Toeplitz matrices and developed a technique known as *simple-loop method* (SLM), providing individual asymptotic expansions for their eigenvalues. In the Hermitian case, the SLM evolved from treating Laurent polynomials to handling more general symbols in weighted Wiener algebras W^{α} with different weights α. For the non-Hermitian case, the SLM has so far been limited to banded Toeplitz matrices with a fixed number of non-zero diagonals; see [11, 12] for a detailed account.

Let $\lambda_{1,1},\ldots,\lambda_{n,n}$ be the eigenvalues of $T_n(a)$. Under certain assumptions on the symbol a, the SLM shows that there exists an integer $m \geqslant 2$ (depending on the smoothness of a) such that

$$\lambda_{j,n} = \sum_{k=0}^{m-1} \frac{\mathbf{c}_k(\sigma_{j,n})}{(n+1)^k} + E_{n,m}(\sigma_{j,n}),$$

where $\sigma_{j,n} = \pi j/(n+1)$; the coefficients $\mathbf{c}_k : [0,\pi] \to \mathbb{C}$ are functions depending on a that can be computed; and the remainder term $E_{n,m}(\sigma_{j,n})$ is of order $O(n^{-m})$ as $n \to \infty$ uniformly in $j = 1,\ldots,n$. Such expansions have inspired a number of numerical studies (see, e.g. [13–15]), suggesting broader applicability beyond the original simple-loop setting.

In the present work, we focus on general banded Toeplitz matrices, that is, with symbols having the form (1.1). Our attention is on the eigenvalues approaching simple and non-degenerate points of the limiting set. Roughly speaking, these correspond to interior points of the analytic arcs forming the limiting set, and will be described in detail later. We extend SLM to this setting, deriving the respective individual asymptotic eigenvalue expansions.

The paper is organized as follows. Our main results are presented in Section 2. The technical tools needed for the proofs appear in Section 3, while the proofs themselves are given in Section 4. In Section 5, we introduce a numerical algorithm that implements our expansions, and in Section 6, we present several numerical experiments that illustrate our results.

2. MAIN RESULTS

For a Laurent polynomial a with the form (1.1), the limiting set $\Lambda(a)$ of the spectra $\operatorname{sp} T_n(a)$ can be defined as

$$\Lambda(a) = \liminf_{n\to\infty} \operatorname{sp} T_n(a).$$

In [5], P. Schmidt and F. Spitzer gave the following interesting description of $\Lambda(a)$: a point $\lambda \in \mathbb{C}$ belongs to $\Lambda(a)$ if and only if $|z_r(\lambda)| = |z_{r+1}(\lambda)|$, where $z_1(\lambda),\ldots,z_{r+\ell}(\lambda)$ are the roots of the polynomial $a^r(a(z)-\lambda)$, sorted in non-decreasing modulus order. This description served as the theoretical base for the algorithm developed in [7], which produces points in the limiting set without computing any eigenvalue at all. It was also employed recently in [9] to obtain individual eigenvalue expansions for a class of tetradiagonal Toeplitz matrices. We use the same description here.

A point $\lambda \in \Lambda(a)$ is called *simple* if $|z_{r-1}(\lambda)| < |z_r(\lambda)| = |z_{r+1}(\lambda)| < |z_{r+2}(\lambda)|$ but $z_r(\lambda) \neq z_{r+1}(\lambda)$. (In the particular cases $r = 1$, $\ell = 1$, we simply remove the terms $z_{r-1}(\lambda)$, $z_{r+2}(\lambda)$, respectively.) In such a case there is a unique number $\varphi \in (-\pi,\pi]\backslash\{0\}$ such that $z_{r+1}(\lambda)/z_r(\lambda) = e^{i\varphi}$. In the bulk of our calculation we will need to find the rth root of the polynomial $z^r(a(z) - a(e^{is}z))$ as a function of s, which according to the implicit function theorem, can be done locally if

$$\frac{dz}{ds} = \frac{ie^{is}za'(e^{is}z)}{a'(z) - e^{is}a'(e^{is}z)}$$

exists and is non zero. Hence, we call a simple point λ *non-degenerate* if

$$a'(z_r(\lambda)) - e^{i\varphi}a'(e^{i\varphi}z_r(\lambda)) \neq 0,$$

and otherwise we call it *degenerate*. According to Theorem 3.2 in [7], a non-degenerate simple point is a regular point of $\Lambda(a)$, meaning that it has an open neighborhood $U \subset \mathbb{C}$ such that $\Lambda(a) \cap U$ is an analytic arc (without self-intersection) starting and ending at the boundary of U.

Let λ_0 be a non-degenerate simple point of $\Lambda(a)$, and let $U \subset \mathbb{C}$ be a neighborhood of λ_0 such that

$$|z_1(\lambda)| \leqslant \ldots \leqslant |z_{r-1}(\lambda)| < |z_r(\lambda)| = |z_{r+1}(\lambda)| < |z_{r+2}(\lambda)| \leqslant \ldots \leqslant |z_{r+\ell}(\lambda)|, \tag{2.1}$$

for every $\lambda \in U \cap \Lambda(a)$. Since λ_0 is a regular point of $\Lambda(a)$, we must have $a'(z_r(\lambda_0)) \neq 0$, and, by reducing U if necessary, we can assume that the same is true for every $\lambda \in U \cap \Lambda(a)$.

Since $U \cap \Lambda(a)$ is an analytic arc, the inverse function theorem tells us that each z_j is analytic there also. Hence, we can extend each z_j analytically to all of U.

If λ runs over the analytic arc $U \cap \Lambda(a)$, the number $\varphi(\lambda)$ satisfying

$$\frac{z_{r+1}(\lambda)}{z_r(\lambda)} = e^{i\varphi(\lambda)}$$

is unique and real. Note that by swapping $z_r(\lambda)$ with $z_{r+1}(\lambda)$, if necessary, we can assume that $\varphi(\lambda) \in (0, \pi]$. Naturally, φ becomes an analytic function on $U \cap \Lambda(a)$, and we can extend it analytically to all of U, but now it will have complex values. We will prove that φ have an inverse function ψ, which is a conformal map. Finally, consider the function $u : \varphi(U) \to z_r(U)$ given by $u(s) = z_r \circ \psi(s)$, which is clearly analytic. See the following diagram.

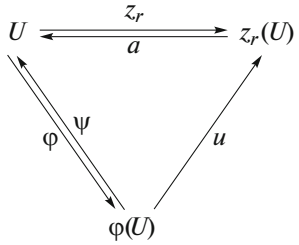

Fix a non-degenerate simple point $\lambda_0 \in \Lambda(a)$ and let $s_0 = \varphi(\lambda_0)$; consider the set

$$\Pi_n = \{s \in \mathbb{C} : s_0 - \alpha \leqslant \Re(s) \leqslant s_0 + \beta, |\Im(s)| \leqslant M/n\},$$

where $M > 0$ is a sufficiently large constant and $\alpha, \beta > 0$ are chosen so that

- $s_0 - \alpha \geqslant 0$ and $s_0 + \beta \leqslant \pi$;
- for every sufficiently large n, u admits an analytic continuation on Π_n, and for every $s \in \Pi_n \cap \mathbb{R}$ the point $\lambda = a(u(s))$ satisfies (2.1) and $a'(u(s)) - ie^{is}a'(e^{is}u(s)) \neq 0$.

For $s \in \Pi_n$, let $v_j(s) \equiv z_j(\psi(s))/z_r(\psi(s))$ and define $\theta : \Pi_n \to \mathbb{C}$ as

$$\theta(s) = \begin{cases} \displaystyle\prod_{j=1}^{r-1} \frac{e^{is} - v_j(s)}{1 - v_j(s)} \prod_{j=r+2}^{r+\ell} \frac{1 - v_j(s)}{e^{is} - v_j(s)} & \text{if} \quad r, \ell \geqslant 2; \\ \displaystyle\prod_{j=3}^{1+\ell} \frac{1 - v_j(s)}{e^{is} - v_j(s)} & \text{if} \quad r = 1, \quad \ell \geqslant 2; \\ \displaystyle\prod_{j=1}^{r-1} \frac{e^{is} - v_j(s)}{1 - v_j(s)} & \text{if} \quad \ell = 1, \quad r \geqslant 2; \\ 1 \quad \text{if} \quad r = \ell = 1. \end{cases}$$

Since $\Lambda(a)$ is the limiting set of the spectra $\operatorname{sp} T_n(a)$, for every sufficiently large n, we will have eigenvalues of $T_n(a)$ in U. The following theorem gives us a recursive equation to calculate them.

Theorem 2.1. *Let a be the Laurent polynomial in* (1.1) *and let $\lambda_{l_1,n},\dots,\lambda_{l_\varrho,n}$ be the eigenvalues of $T_n(a)$ belonging to U. Then, for every sufficiently large $n\in\mathbb{N}$ the following statements hold.*

(i) *The numbers $\lambda_{l_1,n},\dots,\lambda_{l_\varrho,n}$ are pairwise distinct and for each $p=1,\dots,\varrho$, there is a number $s_{j_p,n}\in\Pi_n$ such that $\lambda_{l_p,n}=\psi(s_{j_p,n})$.*

(ii) *For each $p=1,\dots,\varrho$, there exist a small neighborhood $\Theta_{j_p,n}$ where $s=s_{j_p,n}$ is the unique solution of*

$$(n+r)s+\eta(s)=2\pi j_p+R_n(s),$$

with $\eta(s)\equiv \mathrm{i}\log\theta(s)$ (where the principal branch of the logarithm is taken) and R_n is an infinitely differentiable function over $\Pi_n\cap\mathbb{R}=[s_0-\alpha,s_0+\beta]$, playing the role of a remainder term with order $R_n(s_{j_p,n})=O(\delta^n)$ for some $\delta\in(0,1)$, as $n\to\infty$ uniformly in j_p.

In practice, the neighborhood U can be taken such that it contains all the non-degenerate simple points of an analytic arc of $\Lambda(a)$. Then ψ will travel through that analytic arc from one end to the other, and the subsequence $(j_p)_{p=1}^{\varrho}$ will have the form $j_p=p_0+p$ for some fixed number p_0. In such a case, the eigenvalues $\lambda_{l_p,n}$ for $p=1,\dots,\varrho$ will be sorted along the respective analytic arc from one end to the other. We use this approach in Section 6 to sort the eigenvalues and to measure the respective errors.

Theorem 2.2. *Under the same hypothesis of Theorem* 2.1*, as $n\to\infty$, for every integer $m\geqslant 1$ and every $p=1,\dots,\varrho$ we have the following expansions:*

$$s_{j_p,n}=\sum_{k=0}^{m-1}\frac{\mathbf{q}_k(\sigma_{j_p,n})}{(n+r)^k}+E_{n,m}(\sigma_{j_p,n}),$$

$$\lambda_{l_p,n}=\sum_{k=0}^{m-1}\frac{\mathbf{r}_k(\sigma_{j_p,n})}{(n+r)^k}+E^*_{n,m}(\sigma_{j_p,n}),$$

where $\sigma_{j_p,n}=2\pi j_p/(n+1)$ and the coefficients $\mathbf{q}_k$ and $\mathbf{r}_k$ are functions that, in principle, can be determined explicitly, for instance

$$\mathbf{q}_0(s)=s,\quad \mathbf{q}_1(s)=-\eta(s),\quad \mathbf{q}_2(s)=\eta(s)\eta'(s);$$

$$\mathbf{r}_0(s)=\psi(s),\quad \mathbf{r}_1(s)=-\psi'(s)\eta(s),\quad \mathbf{r}_2(s)=1/2\psi''(s)\eta^2(s)+\psi'(s)\eta(s)\eta'(s);$$

$E_{n,m}$ and $E^*_{n,m}$ are remainder terms satisfying $E_{n,m}(\sigma_{j_p,n})=O(1/n^m)$ and $E^*_{n,m}(\sigma_{j_p,n})=O(1/n^m)$, as $n\to\infty$ uniformly in j_p.

Our numerical experiments show (see Figs. 5, 9, and 12) that, when approaching the singular points of the limiting set, the accuracy of the expansions in Theorem 2.2 decreases, but remains acceptable if high precision calculations are not required.

3. TECHNICAL MATTERS

Throughout this section we assume that a is a Laurent polynomial with the form (1.1), and that $\lambda_0\in\Lambda(a)$ is a non-degenerate simple point.

Lemma 3.1. *For every sufficiently large n, the function ψ is a conformal map of Π_n onto its image.*

Proof. Since $\psi=a\circ u$, it is clearly analytic. Suppose that there exist $s_1,s_2\in\Pi_n\cap\mathbb{R}=[s_0-\alpha,s_0+\beta]$ such that $\psi(s_1)=\psi(s_2)$. We then have

$$z_j\circ\psi(s_1)=z_j\circ\psi(s_2),$$

for $j=1,\dots,r+\ell$. Consequently, taking $j=r,r+1$ we get

$$z_r\circ\psi(s_1)=z_r\circ\psi(s_2)\quad\text{and}\quad z_{r+1}\circ\psi(s_1)=\mathrm{e}^{\mathrm{i}s_1}z_r\circ\psi(s_1)=\mathrm{e}^{\mathrm{i}s_2}z_r\circ\psi(s_2)=z_{r+1}\circ\psi(s_2),$$

and we arrive at $\mathrm{e}^{\mathrm{i}(s_1-s_2)}=1$. This happens only if $s_1-s_2=2\pi$, which is impossible, or $s_1-s_2=0$, which implies $s_1=s_2$, as desired. We have proved that ψ is injective on $\Pi_n\cap\mathbb{R}$. Finally, for every sufficiently large n, we can extend the same property to Π_n.

Remark 3.1. The function ψ maps the real interval $\Pi_n \cap \mathbb{R} = [s_0 - \alpha, s_0 + \beta]$ into the limiting set $\Lambda(a)$; consequently, it is our *spectral symbol* (the function in the leading term of the respective eigenvalue expansion). We will construct ψ as $a \circ z_r$. Recall that $z_r(\lambda)$ satisfies both $a(z_r(\lambda)) = \lambda$ and $z_{r+1}(\lambda) = e^{is} z_r(\lambda)$ for some $s \in (0, 2\pi]$.

In principle, the parameter s belongs to $(0, 2\pi]$, but if z^* is a solution of $a(z) - a(e^{is}z) = 0$ with $s \in (\pi, 2\pi]$, we obtain

$$a(z^*) = a(e^{i(2\pi-\gamma)}z^*) = a(e^{-i\gamma}z^*),$$

where $\gamma = 2\pi - s \in [0, \pi)$. Thus, z^* also solves $a(z) - a(e^{-i\gamma}z) = 0$.

On the other hand, if z^* solves $a(z) - a(e^{i\gamma}z) = 0$, then $a(z^*) = a(e^{i\gamma}z^*) = a(e^{is}z^*)$, which implies that it is enough to consider values of s in the interval $(0, \pi]$.

In 1990, H. Widom [16] proved the following. Let $z_1, \ldots, z_{r+\ell}$ be the roots of the polynomial $z^r a(z)$. If they are pairwise distinct, then

$$D_n(a) = \sum_J c_J \omega_J^n, \tag{3.1}$$

where $D_n(a) \equiv \det T_n(a)$, the sum runs over all sets $J \subset \{1, \ldots, r + \ell\}$ having cardinality $|J| = \ell$,

$$\omega_J \equiv (-1)^\ell a_\ell \prod_{j \in J} z_j, \quad c_J \equiv \prod_{j \in J} z_j^r \prod_{\substack{j \in J \\ k \in J^c}} \frac{1}{z_j - z_k},$$

and $J^c \equiv \{1, \ldots, r + \ell\} \backslash J$.

Let s be a point in the region Π_n where ψ is analytic and conformal, and take $\lambda = \psi(s)$. As in the previous section, let $z_1(\lambda), \ldots, z_{r+\ell}(\lambda)$ be the roots of the polynomial $z^r(a(z) - \lambda)$ sorted in non-decreasing modulus order. Recall that $z_{r+1}(\lambda) = e^{is} z_r(\lambda)$.

A point in $\Lambda(a)$ is called *branch point* if at least two of the roots $z_j(\lambda)$ ($j = 1, \ldots, r + \ell$) coincide. Since there is a finite number of branch points, by reducing U if necessary, we can assume that there is no branch points in $U \cap \Lambda(a)$. Consequently, the roots $z_j(\lambda)$ are pairwise distinct for all $\lambda \in U \cap \Lambda(a)$. For brevity, write z_j instead of $z_j(\lambda)$. The following theorem gives an asymptotic expression for $D_n(a - \lambda)$.

Theorem 3.2. *For every sufficiently large n and $\lambda = \psi(s)$ with $s \in \Pi_n$, we have*

$$\frac{D_n(a - \lambda)}{\omega_{J_1}^n (z_r z_{r+2} \ldots z_{r+\ell})^r} = \prod_{\substack{j \in J_1 \\ k \in J_1^c}} \frac{1}{z_j - z_k} + e^{i(n+r)s} \prod_{\substack{j \in J_2 \\ k \in J_2^c}} \frac{1}{z_j - z_k} + G_n(s),$$

where G_n is an analytic function on Π_n satisfying $G_n(s) = O(\delta^n)$ for some $\delta \in (0,1)$, as $n \to \infty$ uniformly in s.

Proof. Applying (3.1) to the symbol $a - \lambda = a - \psi(s)$, we obtain an expression for $D_n(a - \lambda)$ where the main contribution for n large enough is given by terms with maximum absolute value of ω_J. We have here exactly two terms ω_{J_1}, ω_{J_2} with this property:

$$J_1 = \{r, r + 2, r + 3, \ldots, r + \ell\} \quad \text{and} \quad J_2 = \{r + 1, \ldots, r + \ell\}.$$

Let $J_1, J_2, \ldots, J_m$ be the collection of all possible subsets of $\{1, \ldots, r + \ell\}$ with cardinality ℓ. Obviously, $m = (r + \ell)!/(r!\ell!)$. We then have $D_n(a - \lambda) = \sum_{k=1}^m c_{J_k} \omega_{J_k}^n$.

We, in particular, obtain

$$c_{J_1}\omega_{J_1}^n = \frac{(-1)^{\ell n} a_\ell^n z_r^{n+r} z_{r+2}^{n+r} \ldots z_{r+\ell}^{n+r}}{\prod\limits_{\substack{j \in J_1 \\ k \in J_1^c}} (z_j - z_k)}, \quad c_{J_2}\omega_{J_2}^n = \frac{(-1)^{\ell n} a_\ell^n z_{r+1}^{n+r} \ldots z_{r+\ell}^{n+r}}{\prod\limits_{\substack{j \in J_2 \\ k \in J_2^c}} (z_j - z_k)}.$$

A simple calculation produces

$$c_{J_1}\omega_{J_1}^n + c_{J_2}\omega_{J_2}^n = (-1)^{\ell n} a_\ell^n (z_r z_{r+2} \dots z_{r+\ell})^{n+r} \left(\prod_{\substack{j\in J_1\\ k\in J_1^c}} \frac{1}{z_j - z_k} + \mathrm{e}^{\mathrm{i}(n+r)s} \prod_{\substack{j\in J_2\\ k\in J_2^c}} \frac{1}{z_j - z_k} \right)$$

$$= \omega_{J_1}^n (z_r z_{r+2} \dots z_{r+\ell})^r \left(\prod_{\substack{j\in J_1\\ k\in J_1^c}} \frac{1}{z_j - z_k} + \mathrm{e}^{\mathrm{i}(n+r)s} \prod_{\substack{j\in J_2\\ k\in J_2^c}} \frac{1}{z_j - z_k} \right).$$

Consequently,

$$\sum_{k=3}^m c_{J_k}\omega_{J_k}^n = D_n(a-\lambda) - c_{J_1}\omega_{J_1}^n - c_{J_2}\omega_{J_2}^n$$

$$= D_n(a-\lambda) - \omega_{J_1}^n (z_r z_{r+2} \dots z_{r+\ell})^r \left(\prod_{\substack{j\in J_1\\ k\in J_1^c}} \frac{1}{z_j - z_k} - \mathrm{e}^{\mathrm{i}(n+r)s} \prod_{\substack{j\in J_2\\ k\in J_2^c}} \frac{1}{z_j - z_k} \right),$$

which can be written as

$$\frac{D_n(a-\lambda)}{\omega_{J_1}^n (z_r z_{r+2} \dots z_{r+\ell})^r} = \prod_{\substack{j\in J_1\\ k\in J_1^c}} \frac{1}{z_j - z_k} + \mathrm{e}^{\mathrm{i}(n+r)s} \prod_{\substack{j\in J_2\\ k\in J_2^c}} \frac{1}{z_j - z_k} + G_n(s),$$

where $G_n(s) \equiv \sum_{k=3}^m c_{J_k}\omega_{J_k}^n / (\omega_{J_1}^n (z_r z_{r+2} \dots z_{r+\ell})^r)$, which clearly is an analytic function on Π_n. To find the order of G_n as $n \to \infty$, note first that, since the region Π_n is compact and the roots $z_j(\psi(s))$ are sorted in non-decreasing modulus order, the number

$$\delta \equiv \sup \left\{ \frac{|z_j(\psi(s))|}{|z_r(\psi(s))|} : s \in \Pi_n,\ j = 1,\dots,r-1 \right\}$$

is strictly positive and smaller than 1.

Additionally, for each $s \in \Pi_n$ the roots $z_j(\psi(s))$ are pairwise distinct, which implies the existence of a constant γ such that

$$|c_{J_k}| \leqslant \gamma,$$

for any $k = 1,\dots,m$. Every J_k with $k \geqslant 3$ must contain an index $j \in \{1,\dots,r-1\}$, then

$$\frac{|\omega_{J_k}|}{|\omega_{J_1}|} \leqslant \delta \quad \text{for} \quad k \geqslant 3,$$

and we arrive at

$$|G_n(s)| \leqslant \frac{(m-2)\gamma\delta^n}{\inf\{|z_r(\psi(s))| : s \in \Pi_n\}^{r\ell}},$$

which implies $G_n(s) = O(\delta^n)$ uniformly in s, proving the theorem.

4. PROOFS OF THE MAIN RESULTS

Proof of Theorem 2.1. We are interested in the eigenvalues of $T_n(a)$ belonging to U, which is equivalent to solving the equation $D_n(a-\lambda) = 0$ for $\lambda \in U$. Since $\Lambda(a)$ is the limiting set of the spectra $\operatorname{sp} T_n(a)$ and U is a neighborhood of the non-degenerate simple point $\lambda_0 \in \Lambda(a)$, we know that $\operatorname{sp} T_n(a) \cap U \neq \varnothing$ for every sufficiently large n. Hence, let $\lambda_{l_1,n},\dots,\lambda_{l_\varrho,n}$ be the eigenvalues of $T_n(a)$ belonging to U.

From Lemma 3.1 we know that ψ is a conformal (and hence injective) map from Π_n to U. By reducing U, if necessary, we can assume that for each $p = 1,\dots,\varrho$, there exists a unique point $s_{j_p,n}$ in Π_n such that $\psi(s_{j_p,n}) = \lambda_{l_p,n}$. This gives us the part (i).

We now prove the part (ii). From Theorem 3.3, $\lambda = \psi(s)$ is an eigenvalue of $T_n(a)$ if and only if

$$0 = \prod_{\substack{j\in J_1\\ k\in J_1^c}} \frac{1}{z_j - z_k} + e^{i(n+r)s} \prod_{\substack{j\in J_2\\ k\in J_2^c}} \frac{1}{z_j - z_k} + G_n(s),$$

which we write as

$$e^{i(n+r)s} = -\frac{\displaystyle\prod_{\substack{j\in J_2\\ k\in J_2^c}} (z_j - z_k)}{\displaystyle\prod_{\substack{j\in J_1\\ k\in J_1^c}} (z_j - z_k)} - G_n(s) \prod_{\substack{j\in J_2\\ k\in J_2^c}} (z_j - z_k).$$

We now simplify the previous quotient of products. Assume first the case $r \geqslant 2$ and $\ell \geqslant 2$. Let $v_j(s) \equiv z_j(\psi(s))/z_r(\psi(s))$. After expanding and simplifying the common terms, the previous relation becomes

$$e^{i(n+r)s} = \theta(s) - G_n(s) \prod_{\substack{j\in J_2\\ k\in J_2^c}} (z_j - z_k) = \theta(s)(1 - \tilde{G}_n(s)),$$

where

$$\theta(s) \equiv \frac{\displaystyle\prod_{j=1}^{r-1} (e^{is} - v_j(s)) \prod_{j=r+2}^{r+\ell} (1 - v_j(s))}{\displaystyle\prod_{j=1}^{r-1} (1 - v_j(s)) \prod_{j=r+2}^{r+\ell} (e^{is} - v_j(s))}, \quad \tilde{G}_n(s) \equiv \frac{G_n(s)}{\theta(s)} \prod_{\substack{j\in J_2\\ k\in J_2^c}} (z_j - z_k).$$

Taking the principal branch of the logarithm we obtain

$$(n + r)s + i \log \theta(s) = 2\pi j - i \log(1 - \tilde{G}_n(s))$$

for $j \in \mathbb{Z}$, and we are left with finding the order of the last term on the right.

Note that θ is clearly analytic, and if $s \in \Pi_n$ with $j < r$, then $|v_j(s)| < 1$, while $|v_j(s)| > 1$ for $j > r + 1$. Thus θ is bounded away from zero in $s \in \Pi_n$ and is also bounded. Therefore, we can choose a continuous branch of the function $\eta(s) = i \log \theta(s)$ in the region Π_n. Moreover, the term $i \log(1 - \tilde{G}_n(s))$ is analytic there.

A simple calculation shows that

$$|\tilde{G}_n(s)| = \left| \frac{G_n(s)}{\theta(s)} \prod_{\substack{j\in J_2\\ k\in J_2^c}} (z_j - z_k) \right| \leqslant \frac{(2|z_{r+\ell}|)^{r\ell} K \delta^n}{\inf\{|\theta(s)| : s \in \Pi_n\}},$$

where $K = (m - 2)\gamma\delta^n / \inf\{|z_r(\psi(s))| : s \in \Pi_n\}^{r\ell}$, meaning $\tilde{G}_n(s) = O(\delta^n)$. Finally, we have

$$|\log(1 - \tilde{G}_n(s))| = \log(1 + O(\delta^n)) = O(\delta^n).$$

The uniqueness of the solution $s = s_{j_p,n}$ on $\Theta_{j_p,n}$ is a consequence of Lemma 4.1. The cases where $r = 1$ or $\ell = 1$, can be proved similarly.

Take any $p \in \{1,\dots,\varrho\}$. Theorem 2.1 tells us, in particular, that $\lambda_{l_{p,n}} = \psi(s_{j_p,n})$ is an eigenvalue of $T_n(a)$, belonging to U, if and only if $s = s_{j_p,n}$ solves

$$s = \sigma_{j_p,n} - \frac{\eta(s)}{n+r} + \frac{R_n(s)}{n+r}, \tag{4.1}$$

where $\sigma_{j_p,n} = 2\pi j_p/(n+r)$. The relation (4.1) is an implicit equation for s, which we will solve using the Banach fixed-point theorem. The term R_n plays the role of a remainder, suggesting the usage of the reduced equation

$$s = \sigma_{j_p,n} - \frac{\eta(s)}{n+r}. \tag{4.2}$$

We now introduce the necessary objects to prove Theorem 2.2. Consider the functions

$$H_{j_p,n}(s) \equiv \sigma_{j_p,n} - \frac{\eta(s)}{n+r} + \frac{R_n(s)}{n+r},$$

$$H^*_{j_p,n}(s) \equiv \sigma_{j_p,n} - \frac{\eta(s)}{n+r}.$$

Note that if $s_{j_p,n}$ and $s^*_{j_p,n}$ are solutions of (4.1) and (4.2), respectively, then we obtain

$$H_{j_p,n}(s_{j_p,n}) = s_{j_p,n} \quad \text{and} \quad H^*_{j_p,n}(s^*_{j_p,n}) = s^*_{j_p,n}. \tag{4.3}$$

Now, we state the following technical lemma.

Lemma 4.1. *For each $p = 1,\dots,\varrho$ and every sufficiently large n, there exists a collection of mutually disjoint neighborhoods $\Theta_{j_p,n}$ such that $s_{j_p,n} \in \Theta_{j_p,n}$ and both $H_{j_p,n}$ and $H^*_{j_p,n}$ are contractive maps on $\Theta_{j_p,n}$.*

The previous lemma is quite similar to Proposition 4.1 in [9], so we omit the proof.

Proof of Theorem 2.2. After Lemma 4.1, the Banach fixed-point theorem tells us that (4.2) has a unique solution $s = s^*_{j_p,n}$ and that we can find it by iteration. Specifically, if $s^{(0)} \in \Theta_{j_p,n}$ then the sequence $s^{(k)}$, given recursively by $s^{(k)} = H^*_{j_p,n}(s^{(k-1)})$ $(k \geqslant 1)$, converges to $s^*_{j_p,n}$.

Since η is analytic on the compact region Π_n, Eq. (4.2) tells us that $s^*_{j_p,n} = \sigma_{j_p,n} + O(1/n)$. Hence, a first iteration produces

$$s^*_{j_p,n} = H^*_{j_p,n}(\sigma_{j_p,n} + O(1/n)) = \sigma_{j_p,n} - \frac{\eta(\sigma_{j_p,n})}{n+r} - \frac{\eta'(\sigma_{j_p,n})}{n+r}O(1/n) = \sigma_{j_p,n} - \frac{\eta(\sigma_{j_p,n})}{n+r} + O(1/n^2).$$

Similarly, a second iteration reads

$$s^*_{j_p,n} = H^*_{j_p,n}\left(\sigma_{j_p,n} - \frac{\eta(\sigma_{j_p,n})}{n+r} + O\left(\frac{1}{n^2}\right)\right) = \sigma_{j_p,n} - \frac{\eta(\sigma_{j_p,n})}{n+r} + \frac{\eta(\sigma_{j_p,n})\eta'(\sigma_{j_p,n})}{(n+r)^2}$$
$$- \frac{\eta''(\sigma_{j_p,n})}{2(n+r)}\left\{-\frac{\eta(\sigma_{j_p,n})}{n+r} + O\left(\frac{1}{n^2}\right)\right\}^2 + O\left(\frac{1}{n^3}\right) = \sigma_{j_p,n} - \frac{\eta(\sigma_{j_p,n})}{n+r} + \frac{\eta(\sigma_{j_p,n})\eta'(\sigma_{j_p,n})}{(n+r)^2} + O\left(\frac{1}{n^3}\right).$$

Continuing this process, for any integer $m \geqslant 1$, we obtain the expansion

$$s^*_{j_p,n} = \sum_{k=0}^{m-1} \frac{\mathbf{q}_k(\sigma_{j_p,n})}{(n+r)^k} + F_{n,m}(\sigma_{j_p,n}),$$

where $\mathbf{q}_1,\dots,\mathbf{q}_{m-1}$ and $F_{n,m}$ are analytic functions on Π_n, and $F_{n,m}(s) = O(1/n^m)$ uniformly in $s \in \Pi_n$.

Now, we estimate the distance between $s_{j_p,n}$ and $s^*_{j_p,n}$. From (4.3), we have

$$|s_{j_p,n} - s^*_{j_p,n}| = \left|\frac{\eta(s^*_{j_p,n}) - \eta(s_{j_p,n})}{n+r} + R_n(s_{j_p,n})\right| \leqslant \frac{|\eta'(\xi)|}{n+r}|s_{j_p,n} - s^*_{j_p,n}| + |R_n(s_{j_p,n})|,$$

for some ξ in $\Theta_{j_p,n}$. Letting $\|\eta'\|_\infty \equiv \sup\{|\eta'(s)| : s \in \Pi_n\} < \infty$, we arrive at

$$|s_{j_p,n} - s^*_{j_p,n}| \leqslant \frac{|R_n(s_{j_p,n})|}{1 - \|\eta'\|_\infty/(n+r)} = O(\delta^n).$$

Consequently, for any integer $m \geqslant 1$, we obtain the expansion

$$s_{j_p,n} = s^*_{j_p,n} + O(\delta^n) = \sum_{k=0}^{m-1} \frac{\mathfrak{q}_k(\sigma_{j_p,n})}{(n+r)^k} + E_{n,m}(\sigma_{j_p,n}),$$

where $E_{n,m}$ is an analytic function on Π_n with $E_{n,m}(\sigma_{j_p,n}) = O(1/n^m)$ uniformly in j_p.

Finally, to obtain the expansion for $\lambda_{l_p,n} = \psi(s_{j_p,n})$, it is enough to apply ψ to the previous expression using its analyticity and the Taylor theorem.

5. AN ALGORITHM TO CALCULATE THE FUNCTION ψ TOGETHER WITH ITS DOMAIN FOR EACH ANALYTIC ARC IN $\Lambda(a)$

The expansions in Theorem 2.2 can be used to directly calculate any eigenvalue of $T_n(a)$ approaching a non-degenerate simple point of $\Lambda(a)$ for an arbitrarily large n, but first we need ψ, for which we do not have an explicit expression.

It is required to select the point $\lambda_0 \in \Lambda(a)$, which is equivalent to selecting an analytic arc there. Consequently, we will have a different function ψ for each analytic arc. The following algorithm achieves this and provides the domain of each function ψ.

This algorithm produces functions ψ for every analytic arc in $\Lambda(a)$ together with their domains.

(i) For a large and fixed integer n, set $\sigma_{j,n} = \pi j/(n+1)$ $(j = 1,\dots,n)$. The sequence $(\sigma_{j,n})_{j=1}^n$ is a regular mesh of the interval $[0,\pi]$. For each $j = 1,\dots,n$, calculate the roots $\nu_{1,j},\dots,\nu_{r+\ell,j}$ of the polynomial $z^r(a(\nu) - a(e^{i\sigma_{j,n}}\nu)$.

(ii) For every $p = 1,\dots,r+\ell$, compute $w_{1,p,j},\dots,w_{r+\ell,p,j}$ (sorted in non-decreasing modulus order) as the roots of the polynomial

$$w^r(a(w) - a(\nu_{p,j})).$$

(iii) According to the work of Schmidt and Spitzer, $a(\nu_{p,j})$ belongs to $\Lambda(a)$ if and only if $|w_{r,p,j}| = |w_{r+1,p,j}|$. Hence, if this condition holds, take the index p such that $a(\nu_{p,j}) \in U$, define $\psi(\sigma_{j,n}) \equiv a(\nu_{p,j})$, and include the point $\sigma_{j,n}$ in the respective domain. Otherwise, exclude $\sigma_{j,n}$.

Remark 5.1. Each iteration in step (i) produces the sets $\{\nu_{1,j},\dots,\nu_{r+\ell,j}\}$. Some roots may be interchanged between iterations. To track them accurately, sort them in non-decreasing modulus order, ensuring the principal argument of $\nu_{k+1,j}/\nu_{k,j}$ is positive whenever $|\nu_{k+1,j}| = |\nu_{k,j}|$.

Notice that when selecting p in step (iii), we are effectively selecting an analytic arc in $\Lambda(a)$.

The previous algorithm provides the values $\psi(\sigma_{j,n})$ and the collection of indexes j such that $\sigma_{j,n} \in \mathrm{dom}(\psi)$, denoted J. Note that the values $\sigma_{j,n}$ for $j \in J$ may form one or more intervals. To obtain $\psi(s)$ for any $s \in \mathrm{dom}(\psi)$, take a large positive integer q and interpolate the data

$$\{(\sigma_{j,q}, \psi(\sigma_{j,q}))\}_{j\in J}.$$

As an illustration of the precedent algorithm consider again the symbol in Fig. 1, that is

$$a(t) = \frac{-1}{t^4} - \frac{3+2i}{t^3} + \frac{i}{t^2} + \frac{1}{t} + 10t + (3+i)t^2 + 4t^3 + it^4, \tag{5.1}$$

which produces a banded Toeplitz matrix with 9 non-zero diagonals. In this case we have $r = 4$ and $\ell = 4$. The limiting set $\Lambda(a)$ contains five analytic arcs.

For $s \in (-\pi,\pi]$, step (i) produces points over the continuous and smooth functions ν_j $(j = 1,\dots,8)$, but, according to step (iii), only a portion of their domains defines ψ. Applying a to these ν_j and restrict-

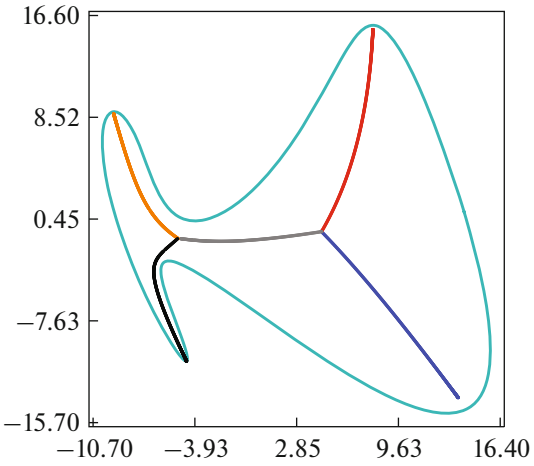

Fig. 2. The range (cyan curve) of the symbol a in (5.1) and the range of ψ_2 (blue), ψ_3 (red), ψ_4 (orange), ψ_5 (gray), and ψ_6 (black).

ing the domains yields the five smooth curves in Fig. 2. It is clear that the limiting set $\Lambda(a)$ is contained in the combined ranges of $a \circ \nu_j$ $(j = 1,\ldots,8)$, to be more specific, put $\psi_j \equiv a \circ \nu_j$ and take into account

$$\operatorname{dom}(\psi_2) \approx (0, 0.1162), \quad \operatorname{dom}(\psi_3) \approx (0, 0.1351), \quad \operatorname{dom}(\psi_4) \approx (2.5446, \pi),$$
$$\operatorname{dom}(\psi_5) \approx (0, 1.6336), \quad \operatorname{dom}(\psi_6) \approx (0, 1.4137),$$

while $\operatorname{dom}(\psi_j) = \varnothing$ for $j = 1, 7, 8$. Note that this domains agree with Remark 3.2. Thus, $\Lambda(a)$ is partitioned into the five analytic arcs given by ψ_j $(j = 2,\ldots,6)$.

6. NUMERICAL EXPERIMENTS

In this section we present our numerical experiments for four selected examples, the first three leading to a tetradiagonal Toeplitz matrix and the last one leading to a pentadiagonal Toeplitz matrix.

As noted in [17], when dealing with spectra of banded Toeplitz matrices, a difficult question arises: how should the eigenvalues be sorted? At first sight, one might be tempted to sort them by the order induced when tracing each analytic arc from endpoint to endpoint. However, when approaching a point where two or more arcs meet, it is very difficult to determine to which arc a particular eigenvalue belongs.

In this article, to measure the error introduced by our expansions, we adopt a different approach. Let us define the following error quantities. For each ψ and each index j_p with $\sigma_{j_p,n} = j_p\pi/(n+1) \in \Pi_n$, consider the mth term approximation given by Theorem 2.2,

$$\lambda_{j_p,n}^{\mathrm{sl}(m)} \equiv \sum_{k=0}^{m-1} \frac{r_k(\sigma_{j_p,n})}{(n+r)^k}, \tag{6.1}$$

and the respective absolute error

$$\mathrm{AE}_{j_p,n}^{\mathrm{sl}(m)} \equiv \operatorname{dist}(\lambda_{j_p,n}^{\mathrm{sl}(m)}, \operatorname{sp} T_n(a)).$$

As the reader can see, by measuring the distance between a point and a set, we avoid any eigenvalue ordering but, at the same time, we make the algorithm heavier. Consider also the respective relative and normalized errors

$$\mathrm{RE}_{j_p,n}^{\mathrm{sl}(m)} \equiv \frac{\mathrm{AE}_{j_p,n}^{\mathrm{sl}(m)}}{|\lambda_{l_p,n}^*|}, \quad \mathrm{NE}_{j_p,n}^{\mathrm{sl}(m)} \equiv \mathrm{AE}_{j_p,n}^{\mathrm{sl}(m)}(n+r)^m,$$

where $\lambda_{l_p,n}^*$ is the eigenvalue of $T_n(a)$ closest to $\lambda_{j_p,n}^{\mathrm{sl}(m)}$.

Table 1. Example 6.1. The relative, absolute, and normalized individual eigenvalue errors $\mathrm{RE}_{j,n}^{\mathrm{sl}(m)}$, $\mathrm{AE}_{j,n}^{\mathrm{sl}(m)}$, and $\mathrm{NE}_{j,n}^{\mathrm{sl}(m)}$, respectively, for $T_n(a)$ with a given by (6.2), $m = 1,2,3$ and different values of n

n	$\mathrm{RE}_n^{\mathrm{sl}(1)}$	$\mathrm{AE}_n^{\mathrm{sl}(1)}$	$\mathrm{NE}_n^{\mathrm{sl}(1)}$	$\mathrm{RE}_n^{\mathrm{sl}(2)}$	$\mathrm{AE}_n^{\mathrm{sl}(2)}$	$\mathrm{NE}_n^{\mathrm{sl}(2)}$	$\mathrm{RE}_n^{\mathrm{sl}(3)}$	$\mathrm{AE}_n^{\mathrm{sl}(3)}$	$\mathrm{NE}_n^{\mathrm{sl}(3)}$
16	3.64×10^{-1}	1.41×10^{-1}	2.40	5.89×10^{-3}	1.07×10^{-2}	3.08	8.07×10^{-4}	3.33×10^{-3}	1.63×10^{1}
32	2.14×10^{-1}	7.40×10^{-2}	2.44	1.73×10^{-3}	2.62×10^{-3}	2.85	9.43×10^{-5}	3.86×10^{-4}	1.39×10^{1}
64	1.09×10^{-1}	3.77×10^{-2}	2.45	4.55×10^{-4}	6.77×10^{-4}	2.86	1.16×10^{-5}	4.73×10^{-5}	1.30×10^{1}
128	5.69×10^{-2}	1.90×10^{-2}	2.45	1.18×10^{-4}	1.70×10^{-4}	2.83	1.44×10^{-6}	5.86×10^{-6}	1.26×10^{1}
256	2.80×10^{-2}	9.55×10^{-3}	2.45	2.92×10^{-5}	4.25×10^{-5}	2.81	1.80×10^{-7}	7.29×10^{-7}	1.24×10^{1}
512	1.41×10^{-2}	4.78×10^{-3}	2.45	7.39×10^{-6}	1.06×10^{-5}	2.80	2.24×10^{-8}	9.11×10^{-8}	1.23×10^{1}
1024	7.06×10^{-3}	2.39×10^{-3}	2.45	1.85×10^{-6}	2.66×10^{-6}	2.80	2.80×10^{-9}	1.14×10^{-8}	1.23×10^{1}
2048	3.53×10^{-3}	1.20×10^{-3}	2.45	4.63×10^{-7}	6.66×10^{-7}	2.79	3.50×10^{-10}	1.42×10^{-9}	1.22×10^{1}

Table 2. Example 6.2. The relative, absolute, and normalized individual eigenvalue errors $\mathrm{RE}_{j,n}^{\mathrm{sl}(m)}$, $\mathrm{AE}_{j,n}^{\mathrm{sl}(m)}$, and $\mathrm{NE}_{j,n}^{\mathrm{sl}(m)}$, respectively, for $T_n(a)$ with a given by (6.2), $m = 1,2,3$ and different values of n. We considered only the eigenvalues $\lambda_{j,n}$ whose distance from the cusp point in Fig. 5 exceeds 1/50

n	$\mathrm{RE}_n^{\mathrm{sl}(1)}$	$\mathrm{AE}_n^{\mathrm{sl}(1)}$	$\mathrm{NE}_n^{\mathrm{sl}(1)}$	$\mathrm{RE}_n^{\mathrm{sl}(2)}$	$\mathrm{AE}_n^{\mathrm{sl}(2)}$	$\mathrm{NE}_n^{\mathrm{sl}(2)}$	$\mathrm{RE}_n^{\mathrm{sl}(3)}$	$\mathrm{AE}_n^{\mathrm{sl}(3)}$	$\mathrm{NE}_n^{\mathrm{sl}(3)}$
16	3.64×10^{-1}	1.41×10^{-1}	2.40	5.89×10^{-3}	1.07×10^{-2}	3.08	8.07×10^{-4}	3.33×10^{-3}	1.63×10^{1}
32	2.14×10^{-1}	7.40×10^{-2}	2.44	1.73×10^{-3}	2.62×10^{-3}	2.85	9.43×10^{-5}	3.86×10^{-4}	1.39×10^{1}
64	1.09×10^{-1}	3.77×10^{-2}	2.45	4.55×10^{-4}	6.77×10^{-4}	2.86	1.16×10^{-5}	4.73×10^{-5}	1.30×10^{1}
128	5.69×10^{-2}	1.90×10^{-2}	2.45	1.18×10^{-4}	1.70×10^{-4}	2.83	1.44×10^{-6}	5.86×10^{-6}	1.26×10^{1}
256	2.80×10^{-2}	9.55×10^{-3}	2.45	2.92×10^{-5}	4.25×10^{-5}	2.81	1.80×10^{-7}	7.29×10^{-7}	1.24×10^{1}
512	1.41×10^{-2}	4.78×10^{-3}	2.45	7.39×10^{-6}	1.06×10^{-5}	2.80	2.24×10^{-8}	9.11×10^{-8}	1.23×10^{1}
1024	7.06×10^{-3}	2.39×10^{-3}	2.45	1.85×10^{-6}	2.66×10^{-6}	2.80	2.80×10^{-9}	1.14×10^{-8}	1.23×10^{1}
2048	3.53×10^{-3}	1.20×10^{-3}	2.45	4.63×10^{-7}	6.66×10^{-7}	2.79	3.50×10^{-10}	1.42×10^{-9}	1.22×10^{1}

Let $\lambda_{j_1,n},\ldots,\lambda_{j_\varrho,n}$ be the eigenvalues of $T_n(a)$ belonging to U. Finally, consider the respective maximum errors

$$\mathrm{AE}_n^{\mathrm{sl}(m)} \equiv \max\{\mathrm{AE}_{j_p,n}^{\mathrm{sl}(m)} : p = 1,\ldots,\varrho\},$$

$$\mathrm{RE}_n^{\mathrm{sl}(m)} \equiv \max\{\mathrm{RE}_{j_p,n}^{\mathrm{sl}(m)} : p = 1,\ldots,\varrho\},$$

$$\mathrm{NE}_n^{\mathrm{sl}(m)} \equiv \max\{\mathrm{NE}_{j_p,n}^{\mathrm{sl}(m)} : p = 1,\ldots,\varrho\}.$$

Our expansions in Theorem 2.2 tells us that $\mathrm{NE}_n^{\mathrm{sl}(m)} = O(1)$, thus we expect to obtain bounded normalized errors as n increases to infinity. In our examples, they are apparently convergent (see Tables 1–3).

In order to calculate any of the preceding errors, we need $\mathrm{sp}\, T_n(a)$ first. All considered examples produce severely ill conditioned eigenvector matrices, i.e., $\approx 10^{21}$ for $n = 1000$; making their calculation very hard. We used the software Julia with data type ComplexBigFloat-2048, which corresponds approximately to 660 working precision digits. The numerical experiments were conducted on a computer with an AMD Ryzen Threadripper 3970X CPU (2 TB RAM) and with Julia version 1.9.2.a.

Example 6.1. Consider the symbol

$$a(t) = \frac{3+\mathrm{i}}{t} + (3+\mathrm{i})t + t^2. \tag{6.2}$$

Table 3. Example 6.3. The relative, absolute, and normalized individual eigenvalue errors $\mathrm{RE}_{j,n}^{\mathrm{sl}(m)}$, $\mathrm{AE}_{j,n}^{\mathrm{sl}(m)}$, and $\mathrm{NE}_{j,n}^{\mathrm{sl}(m)}$, respectively, for $T_n(a)$ with a given by (6.4), $m = 1,2,3$ and different values of n. We considered only the eigenvalues $\lambda_{j,n}$ whose distance from the branch point in Fig. 9 exceeds 1/20

n	$\mathrm{RE}_n^{\mathrm{sl}(1)}$	$\mathrm{AE}_n^{\mathrm{sl}(1)}$	$\mathrm{NE}_n^{\mathrm{sl}(1)}$	$\mathrm{RE}_n^{\mathrm{sl}(2)}$	$\mathrm{AE}_n^{\mathrm{sl}(2)}$	$\mathrm{NE}_n^{\mathrm{sl}(2)}$	$\mathrm{RE}_n^{\mathrm{sl}(3)}$	$\mathrm{AE}_n^{\mathrm{sl}(3)}$	$\mathrm{NE}_n^{\mathrm{sl}(3)}$
16	3.64×10^{-1}	1.41×10^{-1}	2.40	5.89×10^{-3}	1.07×10^{-2}	3.08	8.07×10^{-4}	3.33×10^{-3}	1.63×10^{1}
32	2.14×10^{-1}	7.40×10^{-2}	2.44	1.73×10^{-3}	2.62×10^{-3}	2.85	9.43×10^{-5}	3.86×10^{-4}	1.39×10^{1}
64	1.09×10^{-1}	3.77×10^{-2}	2.45	4.55×10^{-4}	6.77×10^{-4}	2.86	1.16×10^{-5}	4.73×10^{-5}	1.30×10^{1}
128	5.69×10^{-2}	1.90×10^{-2}	2.45	1.18×10^{-4}	1.70×10^{-4}	2.83	1.44×10^{-6}	5.86×10^{-6}	1.26×10^{1}
256	2.80×10^{-2}	9.55×10^{-3}	2.45	2.92×10^{-5}	4.25×10^{-5}	2.81	1.80×10^{-7}	7.29×10^{-7}	1.24×10^{1}
512	1.41×10^{-2}	4.78×10^{-3}	2.45	7.39×10^{-6}	1.06×10^{-5}	2.80	2.24×10^{-8}	9.11×10^{-8}	1.23×10^{1}
1024	7.06×10^{-3}	2.39×10^{-3}	2.45	1.85×10^{-6}	2.66×10^{-6}	2.80	2.80×10^{-9}	1.14×10^{-8}	1.23×10^{1}
2048	3.53×10^{-3}	1.20×10^{-3}	2.45	4.63×10^{-7}	6.66×10^{-7}	2.79	3.50×10^{-10}	1.42×10^{-9}	1.22×10^{1}

Step (i) of the algorithm in Section 5 yields the three functions ν_1 (blue), ν_2 (red), and ν_3 (black), as shown in the middle image of Fig. 3. However, as seen in the right image, only two of these functions contribute to the limiting set $\Lambda(a)$. In both cases, the corresponding domains are $(0,\pi]$.

Although the eigenvalues can be ordered by non-decreasing real part, the range of ψ_1 runs from right to left, while that of ψ_2 goes from left to right. This reversal in direction complicates the ordering and makes the situation less straightforward.

Figure 4 presents the individual relative errors for all eigenvalues of $T_n(a)$. To data was collected by first considering the eigenvalues approximated by ψ_1, followed by those approximated by ψ_2. In this example, we were able to include the full set of eigenvalues. Table 1 shows the maximum relative, absolute, and normalized errors for various values of n and m.

Example 6.2. Consider the symbol

$$a(t) = \frac{c}{t} + ct + t^2, \tag{6.3}$$

where the constant $c \approx -1.91873 - 0.665582\mathrm{i}$ is chosen so that $\Lambda(a)$ consists of exactly two analytic arcs (see [7]). As in the previous example, step (i) of the algorithm in Section 5 produces three functions: ν_1 (blue), ν_2 (red), and ν_3 (black), shown in the middle image of Fig. 6. However, as seen in the right image, only two of these functions contribute to the limiting set $\Lambda(a)$. In both cases, the domains are $(0,\pi]$.

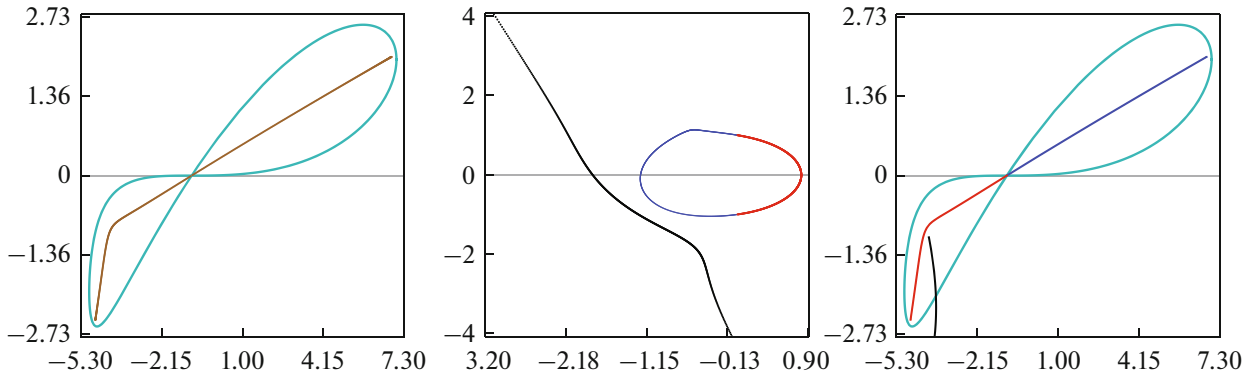

Fig. 3. Example 6.1. Let a be the symbol in (6.2). (Left) the range (cyan curve) and limiting set (brown points). (Middle) The blue, red, and black points are the range of ν_1, ν_2, and ν_3, respectively. (Right) The same as the middle image but for $a \circ \nu_j$.

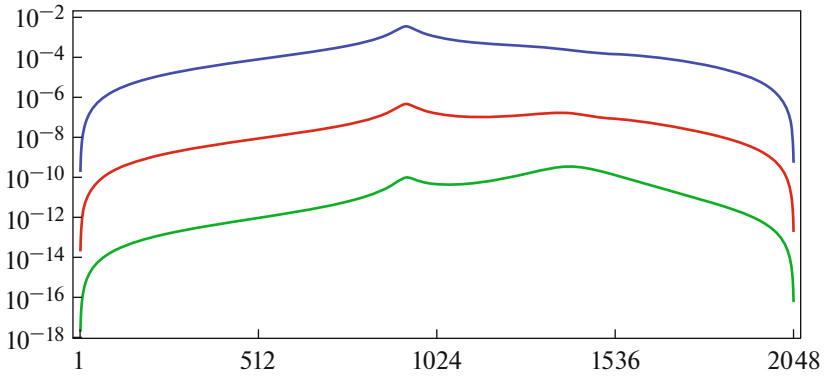

Fig. 4. Example 6.1. The relative error $\mathrm{RE}_{j,n}^{\mathrm{sl}(m)}$ for the eigenvalues of $T_n(a)$ with a given by (6.2), $n = 2048$, and $m = 1$ (blue), $m = 2$ (red), $m = 3$ (green).

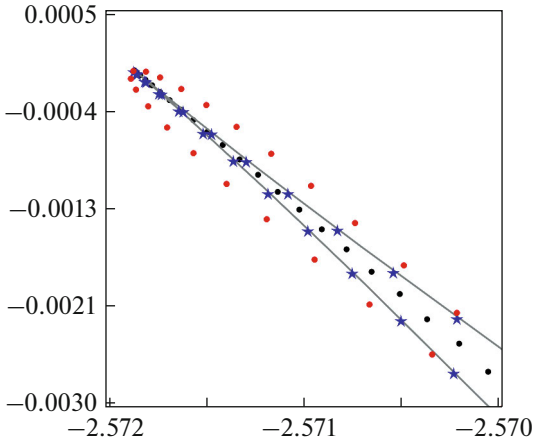

Fig. 5. Example 6.2. A zoom in for the eigenvalues of $T_n(a)$ where a is given by (6.3) and $n = 2048$. The gray curve is the limiting set. The black points are the exact eigenvalues while the blue stars and red points are the eigenvalue approximations $\lambda_{j,n}^{\mathrm{sl}(m)}$ in (6.1), for $m = 1$ and $m = 2$, respectively.

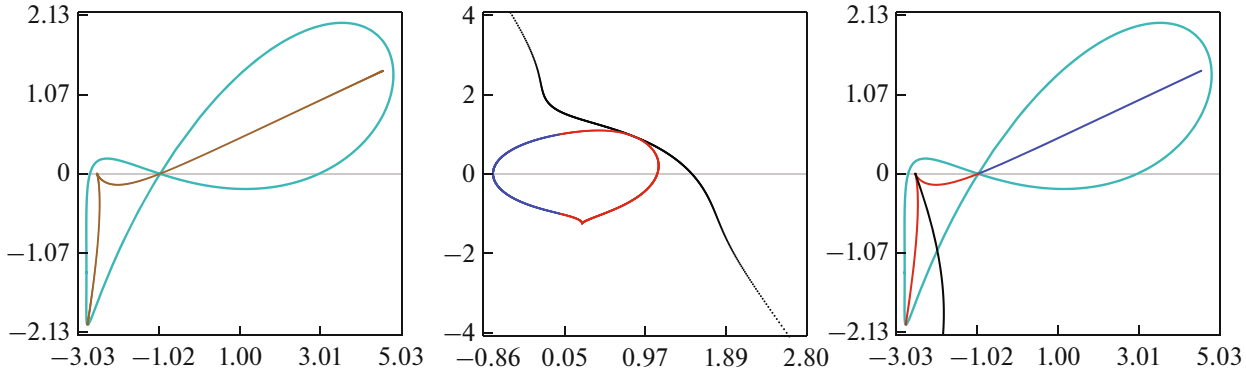

Fig. 6. Example 6.2. Let a be the symbol in (6.3). Left: the range (cyan curve) and limiting set (brown points). Middle: The blue, red, and black points are the range of ν_1, ν_2, and ν_3, respectively. Right: The same as the middle image but for $a \circ \nu_j$.

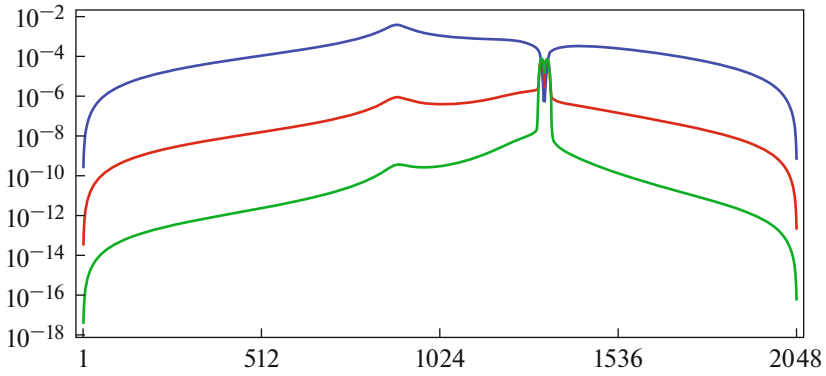

Fig. 7. Example 6.2. The relative error $\mathrm{RE}_{j,n}^{\mathrm{sl}(m)}$ for the eigenvalues of $T_n(a)$ with a given by (6.3), $n = 2048$ and $m = 1$ (blue), $m = 2$ (red), $m = 3$ (green).

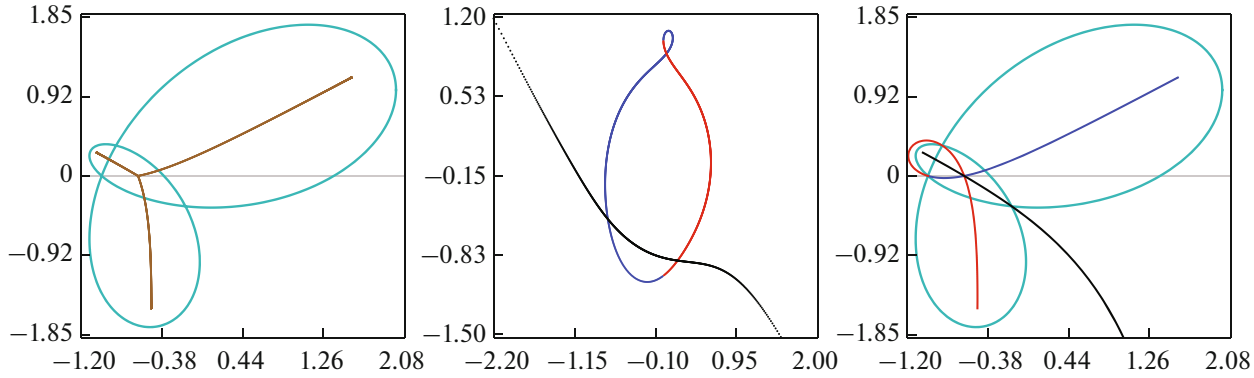

Fig. 8. Example 6.3. Let a be the symbol in (6.4). Left: the range (cyan curve) and limiting set (brown points). Middle: The blue, red, and black points are the range of ν_1, ν_2, and ν_3, respectively. Right: The same as the middle image but for $a \circ \nu_j$.

The presence of a cusp point in the limiting set significantly complicates the ordering of the eigenvalues. Figure 5 shows a zoomed-in view of the eigenvalues near this point. It illustrates how difficult it is to determine whether a given eigenvalue belongs to one arc or the other. Furthermore, near this non-simple point, the approximation with one term $\lambda_{j,n}^{\mathrm{sl}(1)}$ (blue stars) outperforms the two-term approximation $\lambda_{j,n}^{\mathrm{sl}(2)}$ (red points), highlighting that our results are not valid for non-simple points.

Figure 7 displays the individual relative errors for all eigenvalues of $T_n(a)$. To obtain the data, we first worked with the eigenvalues approximated via ψ_1, followed by those approximated via ψ_2. In this example, it was possible to work with the full set of eigenvalues. However, it is worth noting that those located near the cusp point exhibit irregular error behavior. Table 2 presents the maximum relative, absolute, and normalized errors for various values of n and m.

Example 6.3. Consider the symbol

$$a(t) = \frac{3+\mathrm{i}}{t} + (3+\mathrm{i})t + t^2. \tag{6.4}$$

In this case, the limiting set $\Lambda(a)$ consists of three analytic arcs. Step (i) of the algorithm in Section 5 yields the three functions ν_1 (blue), ν_2 (red), and ν_3 (black), as shown in the middle image of Fig. 8. As seen in the right image, all three functions contribute to different portions of the limiting set $\Lambda(a)$. Their respective domains are approximately given by $\mathrm{dom}(\psi_1) \approx (0, 2.8881)$, $\mathrm{dom}(\psi_2) \approx (0, 2.2365)$, and $\mathrm{dom}(\psi_3) \approx (0, 1.1585)$.

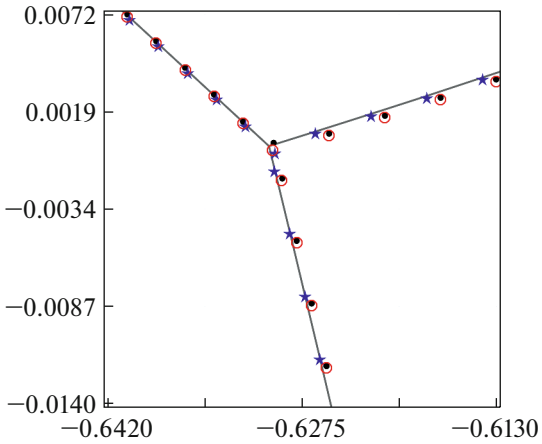

Fig. 9. Example 6.3. A zoom in for the eigenvalues of $T_n(a)$ where a is given by (6.4) and $n = 2048$. The gray curve is the limiting set. The black points are the exact eigenvalues while the blue stars and red points are the eigenvalue approximations $\lambda_{j,n}^{\mathrm{sl}(m)}$ in (6.1), for $m = 1$ and $m = 2$, respectively.

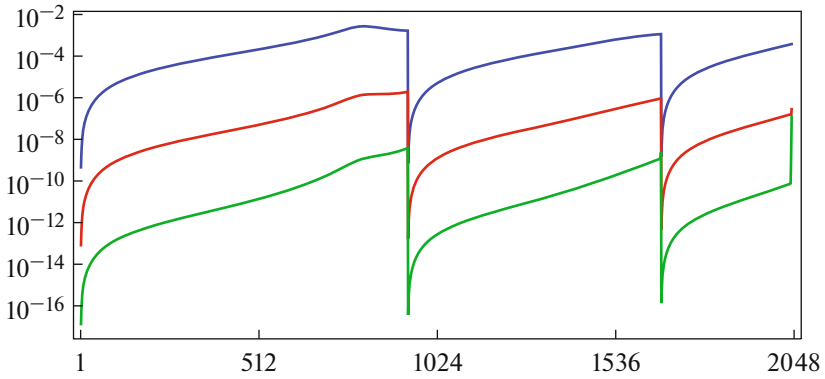

Fig. 10. Example 6.3. The relative error $\mathrm{RE}_{j,n}^{\mathrm{sl}(m)}$ for the eigenvalues of $T_n(a)$ with a given by (6.4), $n = 2048$ and $m = 1$ (blue), $m = 2$ (red), $m = 3$ (green).

Figure 9 shows a zoomed-in view of the eigenvalues and their approximations near the branch point where the three analytic arcs meet, highlighting the eigenvalues and their approximations. Figure 10 presents the individual relative errors $\mathrm{RE}_{j,n}^{\mathrm{sl}(m)}$ for all eigenvalues of $T_n(a)$ and $m = 1$ (blue), $m = 2$ (red), and $m = 3$ (green). The data was obtained by considering first the eigenvalues approximated by ψ_1 (from right to left), followed by those approximated by ψ_2 (from bottom to top), and finally those by ψ_3 (from top to bottom). Table 3 reports the maximum relative, absolute, and normalized errors for various values of n and m.

Example 6.4. Consider the symbol

$$a(t) = \frac{2}{t^2} + \frac{1}{t} + 3t - t^2, \tag{6.5}$$

which generates a penta-diagonal Toeplitz matrix. In this case, the limiting set $\Lambda(a)$ consists of five analytic arcs. Step (i) of the algorithm in Section 5 produces the four functions ν_1 (blue), ν_2 (red), ν_3 (black), and ν_4 (orange), plotted in the middle image of Fig. 11. As shown in the right image, all four functions contribute to different parts of the limiting set $\Lambda(a)$, in particular, ψ_3 gives rise to two different parts. The corresponding domains are approximately given by $\mathrm{dom}(\psi_1) = \mathrm{dom}(\psi_2) \approx (0,1.7449)$, $\mathrm{dom}(\psi_3) \approx (0,0.8975) \cup (1.8015,2.7869)$, and $\mathrm{dom}(\psi_4) \approx (0,0.8975)$.

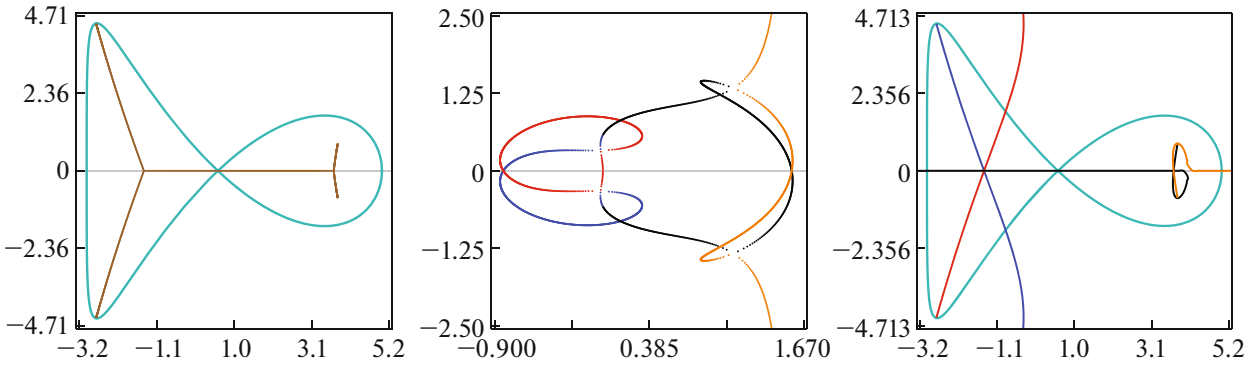

Fig. 11. Example 6.4. Let a be the symbol in (6.5). (Left) The range (cyan curve) and limiting set (brown points). (Middle) The blue, red, black, and orange points are the range of ν_1, ν_2, ν_3, and ν_4, respectively. (Right) The same as the middle image but for $a \circ \nu_j$.

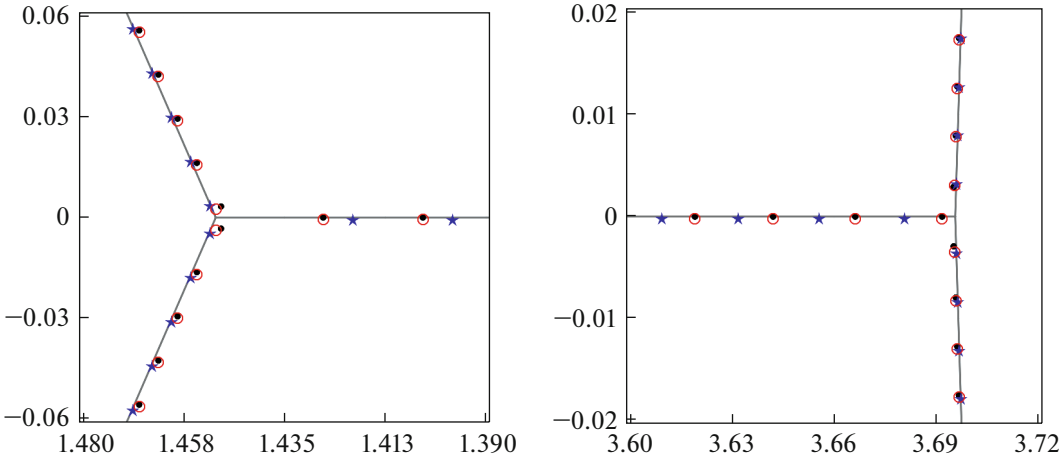

Fig. 12. Example 6.4. A zoom in for the eigenvalues of $T_n(a)$ where a is given by (6.5) and $n = 2048$, near the two branch points where different analytic arcs meet. The gray curve is the limiting set. The black points are the exact eigenvalues while the blue stars and red points are the eigenvalue approximations $\lambda_{j,n}^{sl(m)}$ in (6.1), for $m = 1$ and $m = 2$, respectively.

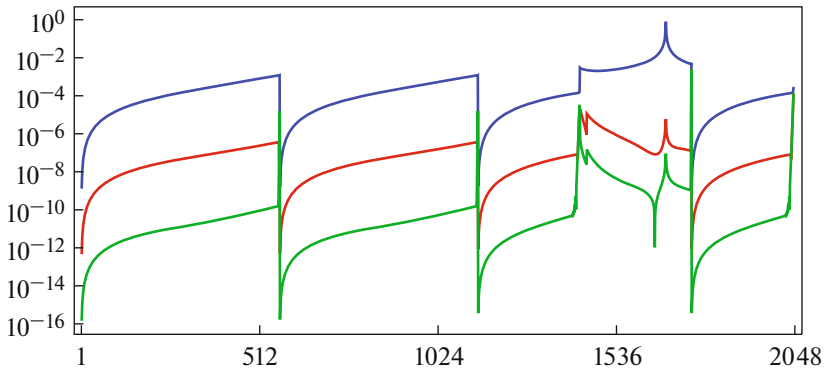

Fig. 13. Example 6.4. The relative error $\mathrm{RE}_{j,n}^{\mathrm{sl}(m)}$ for the eigenvalues of $T_n(a)$ with a given by (6.5), $n = 2048$ and $m = 1$ (blue), $m = 2$ (red), $m = 3$ (green).

Table 4. Example 6.4. The relative, absolute, and normalized individual eigenvalue errors $\mathrm{RE}_{j,n}^{\mathrm{sl}(m)}$, $\mathrm{AE}_{j,n}^{\mathrm{sl}(m)}$, and $\mathrm{NE}_{j,n}^{\mathrm{sl}(m)}$, respectively, for $T_n(a)$ with a given by (6.5), $m = 1,2,3$ and different values of n. We considered only the eigenvalues $\lambda_{j,n}$ whose distance from the two branch points in Figure 12 exceeds 1/20

n	$\mathrm{RE}_n^{\mathrm{sl}(1)}$	$\mathrm{AE}_n^{\mathrm{sl}(1)}$	$\mathrm{NE}_n^{\mathrm{sl}(1)}$	$\mathrm{RE}_n^{\mathrm{sl}(2)}$	$\mathrm{AE}_n^{\mathrm{sl}(2)}$	$\mathrm{NE}_n^{\mathrm{sl}(2)}$	$\mathrm{RE}_n^{\mathrm{sl}(3)}$	$\mathrm{AE}_n^{\mathrm{sl}(3)}$	$\mathrm{NE}_n^{\mathrm{sl}(3)}$
16	2.74×10^{-2}	9.31×10^{-2}	1.58	1.01×10^{-3}	3.45×10^{-3}	1.00	1.18×10^{-4}	4.01×10^{-4}	1.97
32	2.58×10^{-2}	6.83×10^{-2}	2.25	4.46×10^{-4}	1.18×10^{-3}	1.29	8.95×10^{-6}	2.37×10^{-5}	0.85
64	1.43×10^{-2}	3.66×10^{-2}	2.38	1.30×10^{-4}	3.33×10^{-4}	1.41	1.30×10^{-6}	3.32×10^{-6}	0.91
128	8.54×10^{-3}	2.00×10^{-2}	2.58	3.93×10^{-5}	9.22×10^{-5}	1.53	2.09×10^{-7}	4.90×10^{-7}	1.05
256	4.14×10^{-3}	9.92×10^{-3}	2.55	9.61×10^{-6}	2.31×10^{-5}	1.52	2.55×10^{-8}	6.11×10^{-8}	1.04
512	2.10×10^{-3}	5.01×10^{-3}	2.57	2.45×10^{-6}	5.84×10^{-6}	1.54	3.27×10^{-9}	7.80×10^{-9}	1.05
1024	1.04×10^{-3}	2.50×10^{-3}	2.56	6.08×10^{-7}	1.46×10^{-6}	1.53	4.06×10^{-10}	9.74×10^{-10}	1.05
2048	5.26×10^{-4}	1.26×10^{-3}	2.57	1.54×10^{-7}	3.67×10^{-7}	1.54	5.16×10^{-11}	1.23×10^{-10}	1.06

Figure 12 shows a zoomed-in view of the eigenvalues and their approximations near the two branch points where the analytic arcs meet. Figure 13 displays the individual relative errors $\mathrm{RE}_{j,n}^{\mathrm{sl}(m)}$ for all eigenvalues of $T_n(a)$ and $m = 1$ (blue), $m = 2$ (red), and $m = 3$ (green). The data was obtained by first processing the eigenvalues approximated by ψ_1 (from top to bottom), followed by those by ψ_2 (from bottom to top), then the two parts of ψ_3, and finally those by ψ_4 (from bottom to top). Table 4 reports the maximum relative, absolute, and normalized errors for various values of n and m.

FUNDING

The research of M. Bogoya was supported by project CI 41701, Facultad de Ciencias, Universidad del Valle.

The research of S.M. Grudsky was supported by CONACYT (Mexico) project "Ciencia de Frontera" FORDECYT-PRONACES/61517/2020 and by Regional Mathematical Center of the Southern Federal University with the support of the Ministry of Science and Higher Education of Russia, Agreement 075-02-2025-1720.

CONFLICT OF INTEREST

The authors of this work declare that they have no conflicts of interest.

REFERENCES

1. E. E. Tyrtyshnikov, "A unifying approach to some old and new theorems on distribution and clustering," Linear Algebra Appl. **232**, 1–43 (1996).
2. A. Böttcher and S. M. Grudsky, *Spectral Properties of Banded Toeplitz Matrices* (SIAM, Philadelphia, Pa., 2005).
3. A. Böttcher and B. Silbermann, *Analysis of Toeplitz Operators*, 2nd ed. (Springer, Berlin, 2006).
4. U. Grenander and G. Szegő, *Toeplitz Forms and Their Applications*, 2nd ed. (AMS Chelsea, New York, 1984).
5. P. Schmidt and F. Spitzer, "The Toeplitz matrices of an arbitrary Laurent polynomial," Math. Scand. **8**, 15–38 (1960).
6. A. Böttcher and B. Silbermann, *Introduction to Large Truncated Toeplitz Matrices* (Springer-Verlag, New York, 1999).
7. A. Böttcher, J. Gasca, S. M. Grudsky, and A. V. Kozak, "Eigenvalue clusters of large tetradiagonal Toeplitz matrices," Integr. Equations Oper. Theory **93**, 8 (2021).
8. J. L. Ullman, "A problem of Schmidt and Spitzer," Bull. Am. Math. Soc. **73**, 883–885 (1967).
9. M. Bogoya, J. Gasca, and S. M. Grudsky, "Eigenvalues for a class of non-Hermitian tetradiagonal Toeplitz matrices," J. Spectral Theory **15** (1), 441–477 (2025).
10. A. Böttcher, S. M. Grudsky, and E. A. Maximenko, "Inside the eigenvalues of certain Hermitian Toeplitz band matrices," J. Comput. Appl. Math. **233** (9), 2245–2264 (2010).
11. A. Böttcher, M. Bogoya, S. M. Grudsky, and E. A. Maximenko, "Asymptotics of eigenvalues and eigenvectors of Toeplitz matrices," Sb. Math. **208** (11), 1578–1601 (2017).

12. M. Bogoya, A. Böttcher, and S. M. Grudsky, "Asymptotic eigenvalue expansions for Toeplitz matrices with certain Fisher–Hartwig symbols," J. Math. Sci. **271**, 176–196 (2023).
13. S.-E. Ekström, C. Garoni, and S. Serra-Capizzano, "Are the eigenvalues of banded symmetric Toeplitz matrices known in almost closed form?," Exp. Math. **27** (4), 478–487 (2018).
14. S.-E. Ekström and C. Garoni, "A matrix-less and parallel interpolation–extrapolation algorithm for computing the eigenvalues of preconditioned banded symmetric Toeplitz matrices," Numer. Algorithms **80**, 819–848 (2019).
15. S.-E. Ekström and P. Vassalos, "A matrix-less method to approximate the spectrum and the spectral function of Toeplitz matrices with real eigenvalues," Numer. Algorithms **89**, 701–720 (2022).
16. H. Widom, "Eigenvalue distribution of nonselfadjoint Toeplitz matrices and the asymptotics of Toeplitz determinants in the case of nonvanishing index," in *Topics in Operator Theory: Ernst D. Hellinger Memorial Volume* (Birkhäuser, Basel, 1990), pp. 387–421.
17. M. Bolten, S.-E. Ekström, I. Furci, and S. Serra-Capizzano, "Toeplitz momentary symbols: Definition, results, and limitations in the spectral analysis of structured matrices," Linear Algebra Appl. **651**, 51–82 (2022).